Performance of the MISR Instrument During Its First 20 Months in Earth Orbit

David J. Diner, *Associate Member, IEEE,* Jewel C. Beckert, Graham W. Bothwell, and José I. Rodriguez

***Abstract*—The Multi-angle Imaging SpectroRadiometer, one of five science instruments aboard NASA's Terra spacecraft, was launched into earth orbit in December 1999. Acquisition of earth imagery began in February 2000, and the quality of the data is excellent. Overall, MISR has been performing superbly, though the instrument exhibits several idiosyncrasies, some of which were anticipated prior to launch. Details regarding the in-flight performance of the instrument system are presented.**

***Index Terms*—Earth, imaging, multiangle, remote sensing.**

I. Introduction

NASA'S Earth Observing System (EOS) Terra spacecraft (formerly EOS-AM1) was launched on December 18, 1999 from Vandenberg Air Force Base in California. One of Terra's five science instruments is the Multi-angle Imaging SpectroRadiometer [1]. MISR incorporates nine separate pushbroom cameras that acquire moderately high-resolution imagery over a wide angular range in the along-track direction (see Fig. 1). The instrument and the algorithms developed to process its data represent a revolutionary approach to global remote sensing of geophysical and biophysical parameters.

Data from wide field-of-view cross-track scanners have historically been used to build up statistical directional "signatures" of terrestrial scenes through multitemporal compositing [2]. In contrast, data from along-track sensors such as MISR on Terra; the Along-Track Scanning Radiometer (ATSR)-2 on the European Remote Sensing satellite ERS-2 [3]; and the Polarization and Directionality of the Earth's Reflectances (POLDER) instrument on the Japanese Advanced Earth Observing Satellite (ADEOS) [4] offer near-simultaneous multiangle views of terrestrial scenes within minutes as the spacecraft passes over each target. Of these instruments, MISR provides the highest spatial resolution (275 m), and largest view angle range (up to 70.5° from the vertical both forward and backward of nadir).

Prior to Terra launch, the role of multiangle remote sensing in addressing several key science questions was discussed in [5]. With the advent of actual MISR data, the novel applications of moderate spatial resolution multiangle imaging are being explored in detail, and this special issue of the IEEE TRANSACTIONS ON GEOSCIENCE AND REMOTE SENSING includes examples of this research. In this paper, we provide an overview of the in-flight performance of the MISR instrument during the period of December 1999 to August 2001. Along with a brief instrument description, the activation sequence and specific findings regarding MISR's in-flight behavior are described in Sections II and III. We concentrate on the behavior of the instrument system, touching upon aspects of its mechanical, thermal, electronic, and optical performance. Quantitative details regarding radiometric and geometric calibration are not delved into at any length as they are covered in considerable depth in companion papers [6]–[8]. Conclusions are given in Section IV.

Manuscript received September 7, 2001; revised April 16, 2002. This work was supported by a contract with the National Aeronautics and Space Administration and was carried out at the Jet Propulsion Laboratory, California Institute of Technology.

The authors are with the Jet Propulsion Laboratory, California Institute of Technology, Pasadena, CA 91109 USA (e-mail: David.J.Diner@jpl.nasa.gov).

Publisher Item Identifier 10.1109/TGRS.2002.801584.

II. Mission Activation

A. Instrument Overview

The MISR instrument was built by the Jet Propulsion Laboratory for NASA. Details of its design are provided in [1], so only a brief overview is provided here. The fore–aft cameras are paired in a symmetrical arrangement at a fixed set of view angles. Relative to the earth's surface, the along-track angles are nominally 0° (nadir) for the An camera, and 26.1°, 45.6°, 60.0°, and 70.5° forward and backward of nadir for the Af/Aa, Bf/Ba, Cf/Ca, and Df/Da cameras, respectively. Focal lengths of the MISR lenses vary with view angle in order to preserve cross-track sample spacing. MISR contains 36 parallel signal chains corresponding to four spectral bands (446, 558, 672, and 866 nm) in each of the nine cameras. Each signal chain contains the output from 1504 photo-active pixels in four separate charge-coupled device (CCD) line arrays, one for each spectral band. The spacing between the line arrays causes certain bands to "lead" others in spatial position on the ground (see Fig. 1); coregistration of the data in both band and angle is accomplished in ground data processing [8], [9]. From the 705-km orbit of the Terra spacecraft, the swath width is 376 km in the nadir and 413 km off-nadir. The width of the zonal overlap swath (that is, the swath seen in common by all nine cameras along a line of constant latitude) provides multiangle coverage of an entire latitude circle in nine days at the equator, and two days near the poles.

Custom digital circuits used in the system electronics include logic to enable buffering the CCD data to provide 2 sample $\times$ 2 line, 4 sample $\times$ 4 line, or 1 sample $\times$ 4 line averages, in addition to the configuration in which pixels are sent with no averaging (1 sample $\times$ 1 line). The averaging capability is individually selectable within each of the 36 channels, and provides a means of conserving data rate. The system electronics also provide an additional form of data compression by reducing the 14-bit camera outputs to 12 bits through a digital look-up

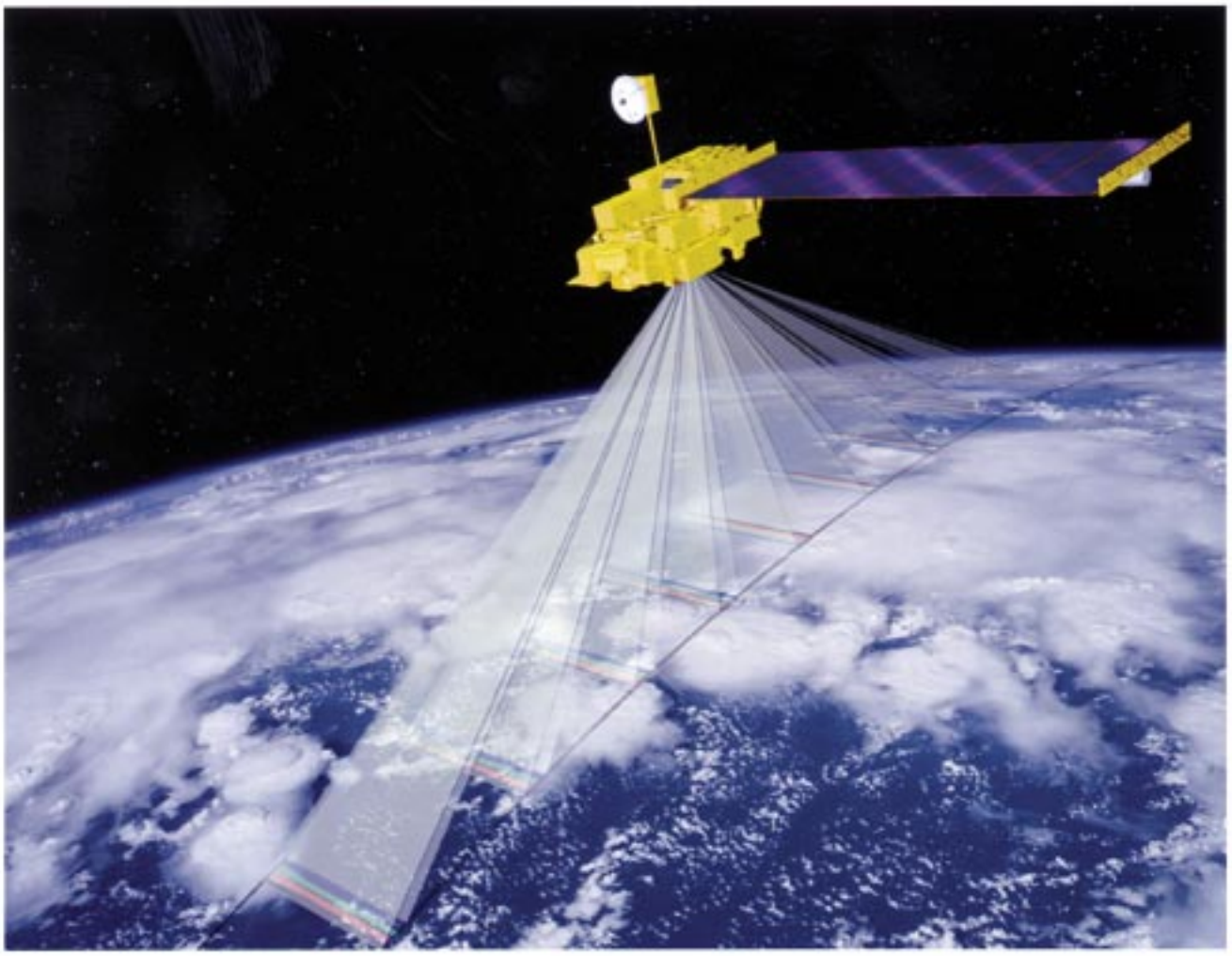

Fig. 1. This graphic illustrates the measurement approach of the MISR instrument. Nine pushbroom cameras point at discrete angles along the spacecraft ground track, and data in four spectral bands are obtained for each camera. It takes 7 min for a point on the earth to be observed at all nine angles.

table that square-root encodes the data numbers. Reversal of the square-root encoding takes place during the early stages of ground data processing.

B. Launch and Orbital Ascent

Terra was launched on an Atlas IIAS rocket at 10:57:39 a.m. Pacific Standard Time (PST) on December 18, 1999, 10 s before the close of the launch window. This down-to-the-wire timing followed last-minute reprogramming of the on-board computers to adjust for high-altitude winds. Separation of the spacecraft from the launch vehicle occurred on schedule about 14 min after launch, and deployment of the solar array occurred 26 min later. MISR survival heaters were turned on around noon PST, and the spacecraft High Gain Antenna (HGA) was deployed in the afternoon. Given that the Terra launch occurred late in the launch window, equator-crossing time on the descending node was about 10:45 a.m. during the first year of operations, putting Terra about one-half hour behind Landsat 7.

On December 21, 1999, MISR was powered on. Unlatching the instrument cover was unsuccessful on the first attempt due to a procedural error in the precanned command sequence that applied power to the wax thermal actuators. This was corrected, and successful unlatching of the instrument cover and deployable calibration panels occurred on the next day. Eight days later three telemetry monitors (TMONs) were activated to provide "watchdog" functions that automatically safeguard the instrument in the event of unexpected temperature, electrical, or computer telemetry readings. On January 5, each of MISR's nine cameras was turned on, and the focal plane and optical bench heaters were activated with set points of 24 °C and 34 °C, respectively. These high temperatures were established to facilitate contaminant bake-out (also known as outgassing). Although the cameras were electrically active, MISR was operating under instructions from the Programmable Read-only Memory (PROM), and the acquisition of image data and use of the high-rate TAXI (Transparent Asynchronous Transmitter–Receiver Interface) link would not be available until after upload of the flight software program to the instrument's computer.

The first full ascent burn to achieve Terra's final orbit took place on January 11, 2000 but was automatically aborted about 1 min into the planned 8.5-min sequence when guidance, navigation, and control (GNC) telemetry detected an excessive rate of

change of spacecraft roll. Later troubleshooting suggested that a plume from one of the thrusters was impinging on the solar array and providing an additional torque on the spacecraft. Additional work to improve the performance of the propulsion system controller was also accomplished. During the subsequent ascent burns, the solar array was oriented to minimize induced torque, and final orbit was achieved on February 23. Terra's orbit is near-polar and sun-synchronous. The Landsat Worldwide Reference System-2 (WRS-2) numbering system is used to identify the 233 orbit "paths" making up each 16-day global repeat cycle. Paths 1–233 progress systematically from east to west, and path 1 crosses the equator at 64.60°W longitude. Orbits are identified with a sequentially incrementing number, and successive orbits are spaced 16 paths apart. Since achieving final orbit, the correspondence between path and orbit numbers is given by the equation $path = \mathrm{mod}_{233}[16 \bullet orbit - 15\,900]$. During the ascent phase of Terra orbital operations, this equation does not apply.

C. Electrical and Thermal Performance

The MISR 1750A flight computer communicates with the Terra spacecraft through 1553-type interfaces for all commanding, instrument housekeeping data transmittal, flight software loading, and memory readout. The system electronics provide the high-rate data interface, as well as camera, power, and mechanism controls. The computers and system electronics are redundant, having an A side and a B side, to reduce the possibility of a single-point failure. Since launch, MISR has been operating exclusively on the A side. Instrument voltages and currents have been routinely monitored throughout the mission, and electrical readings have been performing at the expected levels established during prelaunch testing. A 3% variation in the 120 VDC voltage supplied by Terra is observed when the spacecraft cycles between the solar array and the batteries as the source of power. MISR's instrument power supply contains circuitry to convert the input voltage to a 28 VDC output, along with regulators to maintain this output at a uniform level. A compensating increase in the current being drawn by MISR is observed at the same time the voltage supplied by the spacecraft drops, indicating that MISR's power supply regulators perform as expected.

Details of the MISR thermal performance in flight are provided in [10]. In this paper, a few additional items regarding thermal performance are briefly noted. The outgassing period was originally intended to last for two weeks but was extended through the month of January 2000 due to the delayed orbit ascent maneuvers. During this period, the instrument's optical bench, a monolithic block of aluminum, was thermally unregulated and free to respond to external inputs. The mean flux absorbed by the instrument increases by 34% on the day side due to earth albedo and direct solar heating. Even though this represents a large increase, the optical bench exhibited temperature variations of only ± 0.5 °C owing to its large thermal mass. The period of these oscillations corresponds to the 98.9-min orbit [see Fig. 2(a)]. Superimposed on this orbital variation is a lower frequency signal with a period of about one day. A rough correlative analysis suggests that the source of this modulation

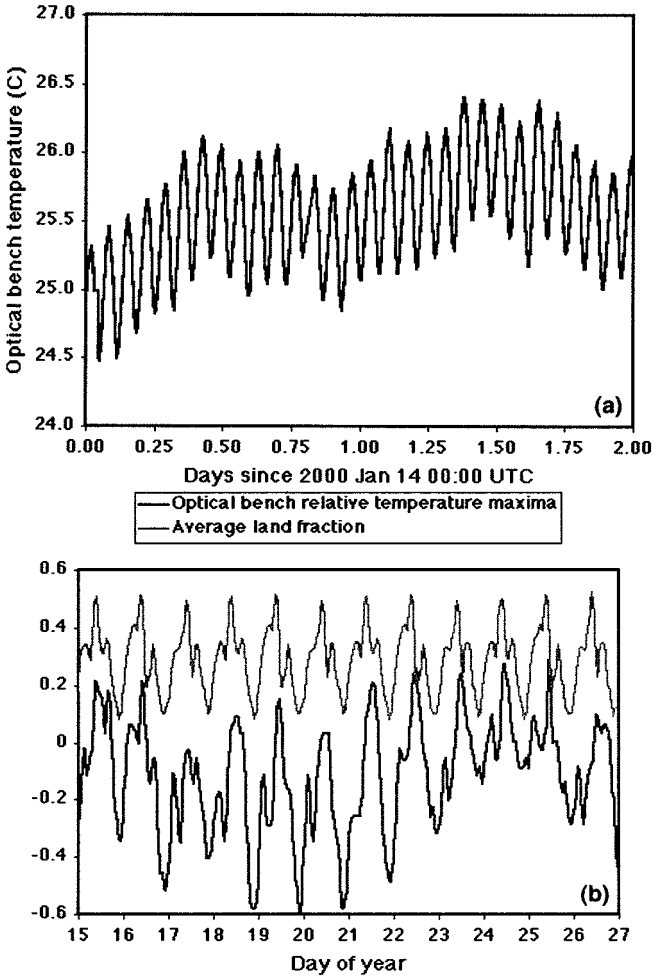

Fig. 2. Measured temperature variations on the MISR optical bench during the outgassing period in January 2000. (a) High temporal resolution plot of optical bench temperature for a two-day period beginning January 14, 2000. (b) Peak orbital temperature versus time for a 12-day period beginning January 15, 2000 (dark line); departures from a typical value of 26.2 °C are shown, and the units on the ordinate are in degrees Celsius. The light line shows land fraction along the spacecraft track averaged over a three-orbit period. For this curve the y-axis is dimensionless.

is a variation in radiative flux between land and ocean, and the near-diurnal nature is due to the fact that Terra returns to approximately the same longitude after one earth day (although not exactly; otherwise, complete global coverage without gaps would not be possible). The orbit-averaged absorbed earth infrared flux is approximately 88% of the total absorbed flux and therefore a more likely candidate than albedo variations for the observed near-diurnal temperature swings. From a simple energy balance calculation, a 3% increase in terrestrial infrared flux results in a 1 °C optical bench temperature increase, given sufficient time to reach thermal equilibrium. It is reasonable to expect earth infrared flux variations of this magnitude when flying over land masses and oceans. Fig. 2(b) shows the peak optical bench temperature reached during each orbit plotted as a function of time, for 12 days beginning January 15, 2000. A constant bias of 26.2 °C has been subtracted from the plotted values. To test the hypothesis that the distribution of land and ocean is responsible for the near-diurnal modulation, we calculated the average land fraction observed along three

successive orbital paths and plotted this value on the same graph. The averaging over three orbits was done to take into account on-orbit experience which shows that it takes many hours for the bench temperatures to stabilize following a step-function change in thermal input. In actuality, the instrument's nadir face integrates radiative flux from the earth over 2π steradians, but to keep the calculations simple we used land fraction averaged along the ground track. Clouds provide a randomly and dynamically varying input, but inclusion of their effects was beyond the scope of this study, and we assumed that to first order they provide a spatially homogenous thermal bias. Fig. 2(b) shows a good correlation between the locations of maximum and minimum values of the peak optical bench temperature and the average land fraction. This analysis suggests that prior to opening the instrument cover, the MISR thermal signature provided a crude but curious characterization of the spatial distribution of the earth's continents.

At launch, the nominal operating plan was to turn the cameras on during the daylight portion of the orbit and turn them off at night to conserve power. However, the associated temperature excursion from day to night is about 13 °C at the camera electronics boards, and it was known prior to launch that the associated thermal cycling would stress these components unduly. Kevlar, with a low coefficient of thermal expansion, was used for the boards, but this measure was deemed insufficient to enable meeting mission life requirements with minimal risk. Provided adequate power margins were available, keeping the cameras powered throughout each orbit would greatly reduce the thermal stresses. After demonstrating that Terra's in-flight performance exhibits adequate power margins, Goddard Space Flight Center approved a plan to leave the MISR cameras continuously powered. New operating modes were designed in which the cameras are powered on but the transmission of camera imagery is inhibited on the night side. Prior to implementing this approach, an interim solution was put into effect in May 2000 whereby the MISR replacement heaters were turned on during the night portion of each orbit. These heaters consume the same power as the camera system, and this approach reduced the day-night temperature excursion to about 8 °C. After extensive testing, new flight software was uploaded to MISR on May 22, 2001. This long-term solution reduces the temperature excursion to about 1 °C, and is expected to extend mission life well beyond the six-year design requirement.

D. "Dark" Imagery

On January 30, 2000 a major milestone was reached with the official end of the MISR outgassing phase and upload of the "at-launch" version of the instrument flight software. Following a memory read-out to verify a proper load, the flight computer was commanded to "jump" from the PROM operating instructions to the flight code. At this point, MISR entered Engineering Mode, which provides voltage, current, temperature, navigation, and status readouts using the now-activated TAXI interface. (Housekeeping telemetry from the low-rate 1553 bus, which was the only source of data until this point, also continued to be available.) During a subsequent contact with the spacecraft, the command to enter Global Mode (the primary science mode) was sent. The nine cameras turned on sequentially as programmed, and MISR began sending science data to Terra's solid-state recorder (SSR). Additionally, the focal plane and optical bench set points were commanded to the nominal operational values of -5 °C and 5 °C, respectively, and the focal plane thermoelectric coolers (TECs) were turned on. Playback of MISR data from the SSR and transmission to the ground commenced at 1:47 p.m. PST. Within two hours, the NASA Langley Atmospheric Sciences Data Center (the Distributed Active Archive Center, or DAAC, at which MISR data are processed) had received the first set of MISR data and sent it to JPL. Because the instrument cover was still closed, the camera data consisted entirely of dark current imagery. The typical signal levels from all nine cameras were similar to the levels observed during prelaunch testing.

Analysis of MISR "dark" imagery revealed an intermittent phenomenon manifested as regularly-spaced tapered vertical stripes, consequently dubbed the "jail bars" [Fig. 3(a)]. These faint, uniformly-spaced vertical stripes showed up at camera turn-on during each orbit (near the northern terminator), progressively got narrower, and finally disappeared after about 20 min. After camera turn-on a rise in instrument electrical current was also seen, and this "extra" current peaked and then decreased over a 20-min period. After some analysis the explanation for the "jail bar" phenomenon was deduced. Because the cameras and their support electronics were powered off during orbit night, the optical bench required additional heating to remain at a constant temperature. The bench is regulated to a constant temperature by heaters that pulse on and off at fixed intervals. The pulse width increases or decreases as more or less heating is required. Turning on the camera electronics adds heat to the bench, gradually reducing the need for heater input. Imperfect electrical isolation permits a tiny cross-talk of the heater pulses into the camera video signal. An on-orbit test confirmed this explanation. Because the magnitude of the additive signal is only one to two data numbers (DN), the signal is drowned out by earthlight during normal imaging operations, although it might be detected in highly stretched imagery acquired near the north terminator.

MISR dark imagery also revealed two effects attributed to passage through the South Atlantic Anomaly (SAA), a dip in the earth's magnetic field caused by an offset and tilt of the geomagnetic axis with respect to the rotation axis. The SAA is a location of enhanced charged particle abundances and extends from South America to the southern tip of Africa, peaking in intensity off the coast of Brazil. The first effect on the imagery consists of random bright points resulting from signals being generated in individual detector elements, most likely by proton radiation (the most abundant particles of the solar wind). These make the images look like a field of faint stars [Fig. 3(b)]. The other effect is manifested in the performance of the line-to-line background stabilization circuitry built into each camera's electronics. If a charged particle event occurs at a particular time, the stabilization circuit can be fooled into thinking the overall background has brightened, and compensates by temporarily decreasing the video offset in several lines of imagery. This effect looks like randomly placed dark horizontal stripes in the images [Fig. 3(c)]. Together, these two phenomena were nick-

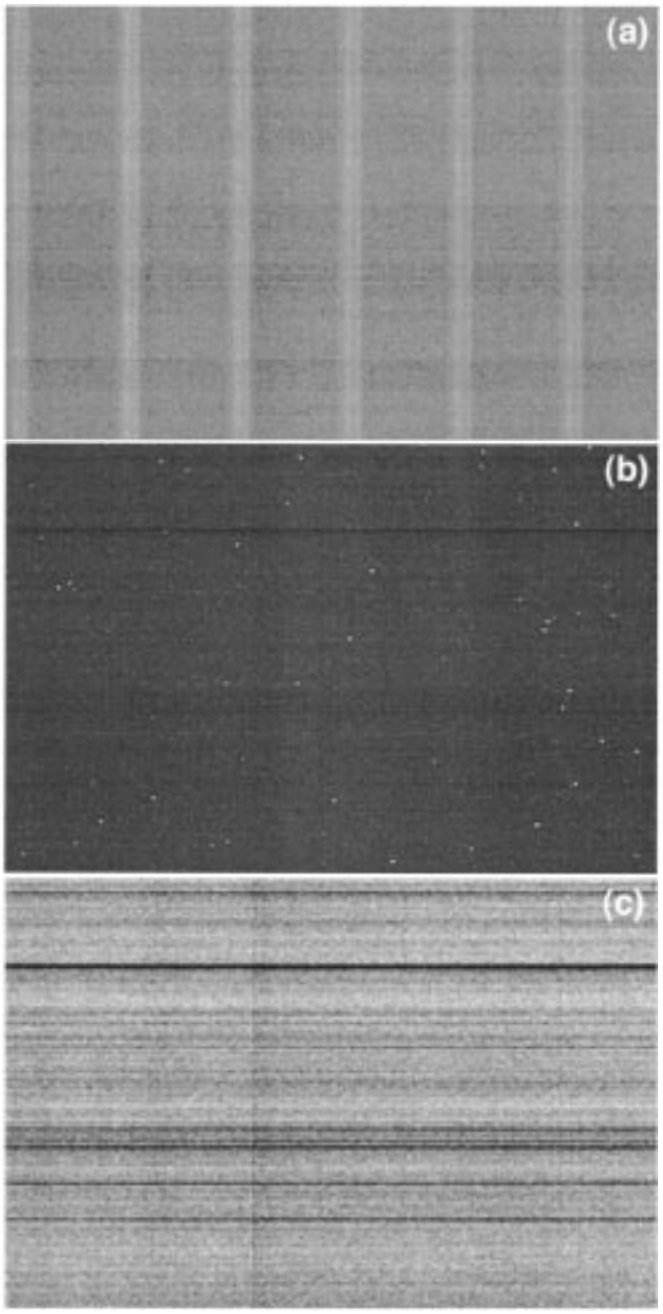

Fig. 3. (a) Example of "jail bars" in red band data of the Df camera, from February 12, 2000 (Terra orbit 821). This signal is due to leakage of optical bench heater pulsing into the camera video and was captured in 41 s of "dark current" data that are displayed here as an image. The vertical stripes are apparent only because the contrast has been greatly enhanced. (b) Example of the "stars," or bright points due to charged particle hits in 41 s dark current imagery of the Df camera red band, from February 12, 2000 (Terra orbit 818) during passage through the South Atlantic Anomaly. (c) Same image as (b) but with an extreme contrast stretch to enhance the "stripes," or variations in the video background level.

named the "stars and stripes." The line-to-line background variations (the "stripes") are typically on the order of 1–2 DN, relative to a typical dark current background of about 350 DN and a full scale value of 16 383 DN (14 bits). The ability to detect these features is a tribute to the low noise of the MISR cameras, and they are not observable in imagery acquired with the cover open.

In contrast to the "stripes," the magnitude of the "stars" varies from several DN above background to thousands of DN (although the larger hits are much less frequent). The relative proportion of hits is small but measurable, varying from about 1 hit (signal level clearly distinguishable from dark current) per 10^6 pixels outside of the SAA to about 1 per 10^3 pixels inside the SAA. A spatial map of the hits, shown in Fig. 4, was generated by gridding the globe into $0.25^\circ \times 0.25^\circ$ cells, and assigning to each cell the maximum DN observed in the red band of the Df camera, for orbits between February 3 and February 16, 2000. Some license has been taken in generating this map since the focal plane data have been map-projected to the earth's surface, which is not strictly valid because the source of the signals is at the spacecraft altitude and the detected events are localized within the 32-mm width of the CCD line arrays. Nevertheless, we took advantage of the map projection software that had been developed for use with earth imagery, and this exercise provided an early operational test of this code. In generating Fig. 4, an approximate compensation was made for the fact that the charged particle signals are associated with the spacecraft position and not the forward-projected location of Df imagery. Individual orbit tracks are visible in the map. Some tracks are not present due to data gaps, missing spacecraft navigation information, or other early-mission processing problems. The locations of the continents have been sketched in graphically. Explanations for the various colors shown in the map are provided in the caption to Fig. 4. In creating the map, the single DN value assigned to each grid cell was culled from hundreds to thousands of pixels in the raw MISR dark imagery, and because each picture element of the map shows the most extreme outlier resulting from proton hits, it accentuates the effect of the charged particle radiation. The result is a representation of the charged particle flux at the Terra orbit altitude, and the SAA shows up clearly. MISR's first geophysical product was generated with the cover closed.

Because occasional hits have a magnitude of thousands of DN, these can affect earth imagery acquired with the cover open. To quantify this effect, data between the equator and 50 °S latitude from orbit 759 (path 220, which crosses the SAA near the location of peak particle flux) were analyzed by generating a histogram of red band data in the Df camera and converting the DN to an "equivalent" reflectance, i.e., the reflectance of a Lambertian target illuminated by overhead sun that would give the same signal as the charged particle "hit." The results are displayed in Fig. 5. "Equivalent" reflectances of a few hundredths due to these hits (comparable to the typical radiometric signal level of midlatitude cloud-free ocean with low aerosol loading) are rare, affecting about 1 pixel in 10^7. Overall, about 0.06% of the pixels have "equivalent" reflectance > 0.004; for latitudes on the same orbit between the equator and 50°N (i.e., outside the SAA) the corresponding value is 0.000 07%, reflecting the three orders of magnitude difference in charged particle flux inside and outside the SAA. Although the SAA effect is small, it is not negligible, though for most applications the effect can be safely ignored, particularly when MISR data are analyzed statistically. Furthermore, certain data filters in MISR higher level processing, such as aerosol

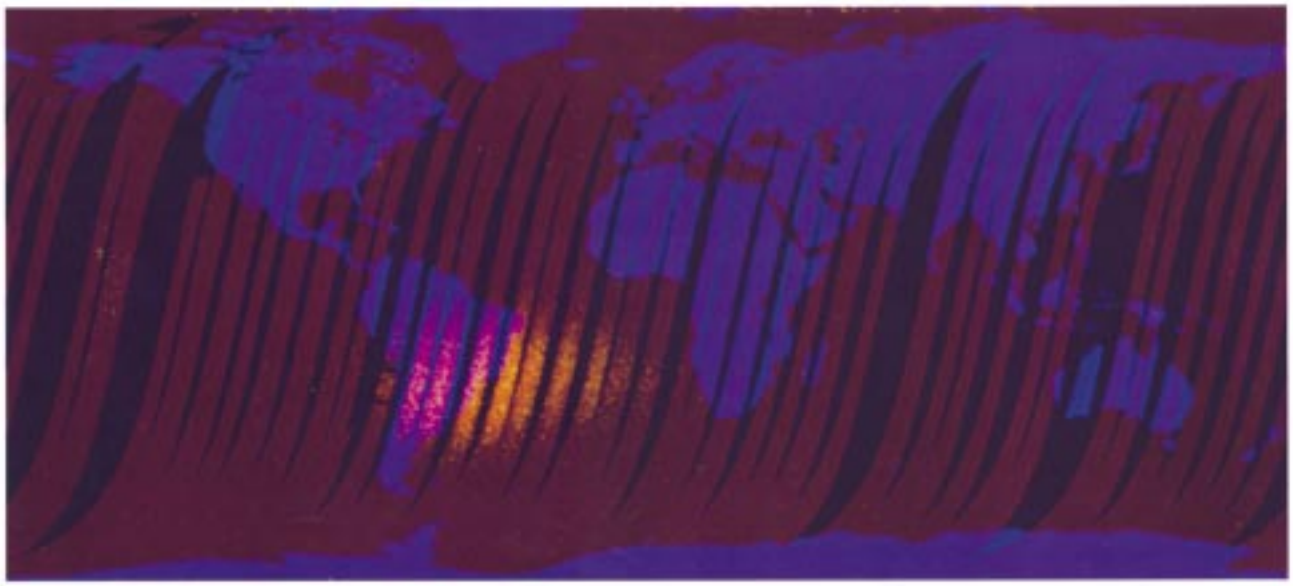

Fig. 4. This map was created by specially processing MISR "dark" data taken between February 3 and February 16, 2000, while the cover was still closed. Data from the red band of the Df camera were geographically projected over a map of earth's land areas. Each picture element is a square measuring 0.25° in latitude and longitude, and shows the most extreme "outlier" resulting from proton hits, accentuating the effect of the South Atlantic Anomaly. Areas with no data are shown in black (over ocean) or blue (over land). Gradations from red to orange represent the strength of the SAA signal over ocean. Over land these colors shift toward purple hues due to mixing with the blue background representing the continental land masses.

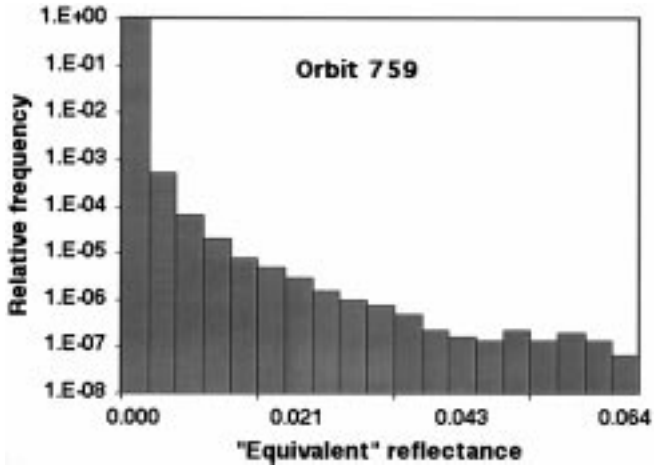

Fig. 5. Relative frequency of proton hits, converted to "equivalent" reflectance, during passage through the South Atlantic Anomaly on Terra orbit 759.

retrievals, safeguard against the use of these corrupted data. At this time, no "despike" algorithm has been implemented in MISR radiometric (Level 1) data processing, and users analyzing imagery in this geographic location should be alert for occasional, isolated bright pixels.

III. Orbital Operations

A. "First Light"

About two months after launch, Terra reached its intended orbit. On the morning of February 24, 2000 at 8:41 a.m. PST, during Terra's 995th orbit of the earth, a command was sent to the MISR instrument to open the instrument's cover. The exceptional "first light" imagery, acquired over James Bay, Canada, arrived at the MISR Science Computing Facility (SCF) later that afternoon.

Fig. 6(a)–(c) show images of James Bay and southern Hudson Bay from the Df, An, and Da cameras, respectively, generated using the cameras' red, green, and blue bands. The increased blue tint at the oblique angles is the result of scattering of light in the atmosphere. Several islands, including the crescent-shaped Akimiski Island, are visible in the frozen bay. Contrast reversals and other color and brightness variations from one angle to another are also apparent, and are likely due to variegated ice textures as well as different angular signatures of cloud and ice. The Df image captures the moment of cover opening, which is represented by the abrupt transition from dark to light near the top of the scene. By the time the An and Da cameras viewed the same area, the cover had been open for several minutes, so the James Bay images from these cameras do not show this transition. This observation highlights the fact that at any one instant, the MISR cameras are not viewing the same point on the ground. However, coregistration of the imagery on a pixel-by-pixel basis is required for the geophysical retrievals. This coregistration is accomplished by using a common map projection and resampling the radiances to this grid, a process known as georectification. Space-Oblique Mercator (SOM) is used for this grid because its projection meridian nominally follows the spacecraft ground track and a constant distance scale is preserved along that track, thus minimizing distortion and resampling effects. The horizontal datum for each projection is the World Geodetic System 1984 (WGS84) ellipsoid.

An unexpected anomaly was discovered in the first-light data. The red, green, and near-infrared data from camera Aa had signal levels significantly lower than all other channels. The faint, but discernible imagery otherwise appeared normal,

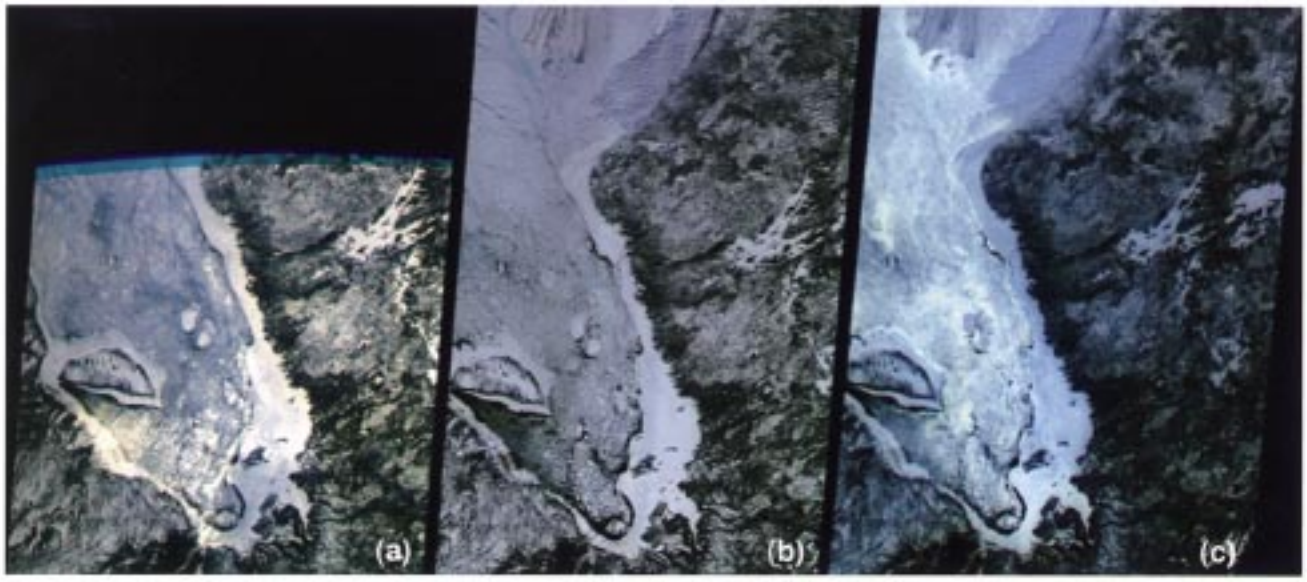

Fig. 6. (a) "First light" image over James Bay, Canada, acquired on Terra orbit 995, February 24, 2000. The dark-to-light transition near the top captures the moment at which the instrument's protective cover was opened. The image is a red, green, blue composite from the Df camera. The data have been resampled to a Space Oblique Mercator projection. (b) Image of the same region acquired on the same orbit by the An camera. (c) Image of the same region acquired on the same orbit by the Da camera.

so we suspected that the 1-s delay between two flight software commands to turn the camera on and to establish the correct exposure times was too short for a particular field programmable gate array (FPGA) to fully power up. A similar phenomenon had been observed in multiple cameras in prelaunch thermal-vacuum testing, at which point the 1-s delay was introduced into the flight software. In orbit, it appeared that the FPGA in Aa was reacting more sluggishly. A successful work-around was established by adding, on each orbit, an extra exposure time command for camera Aa into the absolute time command (ATC) load that is uploaded daily to the spacecraft. Beginning with orbit 1100, this extra command was sent routinely. With the upload of a new flight software version in May 2001, the time delay between the internal camera turn-on and exposure time commands was increased to 8 s for all cameras, and the external ATC command to camera Aa was no longer required.

Evidence of vignetting affecting approximately 75 pixels was seen at the field edges of raw images from the Af and Aa cameras. This is believed to have resulted from a manufacturing error in the sizes of the viewports through which the cameras observe. Indications of such vignetting were present in prelaunch test imagery acquired at the Lockheed-Martin spacecraft integration facility in Valley Forge, PA, but at that point in the program schedule constraints would have precluded corrective action. Because the vignetting surface is out of focus, the response at the field edges is not lost, only reduced in intensity. The effect is also present when the cameras view the instrument's Spectralon flat-field calibration panels, and once the pixel-by-pixel calibration procedures were put in place, the effects of the vignetting were removed from the processed imagery. A minor consequence is some loss in signal-to-noise ratio (SNR) due to the reduced illumination level. However, this is not a significant problem since MISR radiometry has ample SNR margins.

Another feature observed in the imagery from all nine cameras is a faint fringing pattern, with a magnitude of $\sim$1% of the scene illumination level. This fringing is ascribed to interference associated with reflection of light between the CCDs and the spectral filters mounted above them, and had been observed prior to flight. The location of the fringes changes with time, presumably because the physical spacing between the CCDs and filters is temperature sensitive. Bimonthly updates to the pixel-by-pixel calibration coefficients are successful in keeping the magnitude of the fringes at negligible levels for most applications.

B. Data Anomalies

Early in the Terra mission, random occurrences of "bit flips" or transitions from 0 to 1 and vice versa were detected in the header information of MISR data packets. Diagnostics such as an obviously out-of-sequence packet counter or time stamp were used to detect these events. Further investigation showed that similar data errors were showing up in the other Terra high-rate instruments, indicating that the source of the errors was external to the MISR instrument. Because MISR packets are sorted by time and packet sequence counter by the EOS Data and Operations System (EDOS) after receipt on the ground, the bit flips can cause individual packets to be placed out of order. Within limits, postlaunch modifications to the MISR ground data processing software are able to deal with this situation. If an out-of-sequence packet is too far removed from its "true" location, however, the error is not recovered and the resulting MISR imagery has a gap. Radiances in the gap regions are filled in with predefined fill values. There is at least one small gap in almost every swath, and in rare cases, data gaps of many lines have been observed. Detection of bit flips in the imagery (as opposed to header data) is much more difficult, though it is conceivable

that such occurrences are affecting a tiny fraction of the camera data.

Another bit-flip phenomenon, intrinsic to MISR and peculiar to a particular operating configuration of the instrument, was observed in prelaunch testing and affects a small fraction of the imagery. An instrument operating sequence known as Local Mode provides full resolution (1×1 configuration) images in all channels for selected earth targets. This is accomplished by inhibiting pixel averaging in all bands of each of the cameras in sequence, one at a time, beginning with the first camera to acquire the target (Df) and ending with the last camera to view the target (Da). The instrument geometry limits the downtrack length of Local Mode targets to about 300 km. Curiously, during the 60-sec interval when the Ca camera is acquiring full resolution data in all four of its bands, random bit flips occur in the time tags of camera Da's packet headers. Most such occurrences affect the least significant bit, changing the time stamp by 1 msec, though larger errors have been observed, with consequent distortions in the georectified imagery for the Da camera. Local Mode is typically exercised about once per day, thus about 0.1% of the Da camera data are susceptible to this phenomenon. However, the majority of time tags are not corrupted, so the actual proportion of affected data is much smaller.

The MISR instrument occasionally goes "out-of-sync" momentarily if the data rate from the hardware exceeds the flight computer's capacity to appropriately assign packet headers to the image data. This phenomenon was observed in prelaunch testing, and an early plan to operate the blue bands of the C and D cameras in 1×4 averaging configuration was abandoned in order to reduce the instrument data rate and minimize the occurrence of these out-of-sync events. The Global Mode configuration currently in use places all four bands of the nadir camera and the red band of all off-nadir cameras in 1×1 (i.e., no averaging or full resolution), and the remaining bands in 4×4 configuration (1.1-km resolution). Out-of-sync conditions in this configuration are infrequent. During Local Mode sequences, out-of-sync transients occur intermittently. Timing analysis shows that this is caused by the increased data rate and is not a result of the averaging configuration transitions. The ATC Aa camera exposure time command that was in place between March 2000 and May 2001 also intermittently caused out-of-sync conditions. The symptom is that several lines of data in all cameras are simultaneously corrupted, but the instrument has been designed to issue a special data packet indicating that the condition has occurred. Affected image lines are flagged during ground data processing.

Occasional losses of data are associated with recording or transmission anomalies associated with the spacecraft or EDOS data systems. For example, a continuous data outage occurred from June 17–June 20, 2001 due to a single event upset associated with the Terra SSR.

C. Radiometric Calibration

A key component of the MISR On-Board Calibrator (OBC) is a pair of deployable diffuser panels. These are covered with Spectralon, a pure polytetrafluoroethylene (Teflon) polymer resin that is compressed and sintered. While not in use the panels are stowed and protected. Over the north pole, one panel swings backward to reflect diffused sunlight into the fields-of-view of the An, Aa, Ba, Ca, and Da cameras. Over the south pole, the other panel swings forward for calibration of the An, Af, Bf, Cf, and Df cameras. The nadir camera provides a link between the two sets of observations. The diffuse calibration targets are monitored in-flight by multiple *p*, *i*ntrinsic, and *n* doped (PIN) photodiodes and high quantum efficiency (HQE) diodes. The OBC is used to provide camera response as a function of input radiance, as established by the diode detector standards. Ground data processing of the resulting radiometric transfer curves is performed on a per-pixel basis to provide the coefficients for an analytic polynomial equation relating camera data number to radiance. (A quadratic term accounts for small departures from linearity at the low end of the dynamic range.)

In-flight analysis of the relative radiometric response of the calibration diodes between spectral bands of the same diode set and across different diodes showed departures of up to $\sim$10% from the expected performance established preflight. It is suspected that the procedures used for preflight characterizations may not have adequately accounted for out-of-band response, and an attempted preflight system level test of their response did not provide adequate illumination levels to enable a meaningful measurement. Fortunately, the diodes are temporally stable to the few percent level, with the HQE diode chosen as the in-flight stability standard showing about a 1% response change over the course of a year [6]. The diodes therefore remain an essential part of the instrument radiometric calibration subsystem. Greater reliance on alternative procedures to establish the absolute radiometric scale, including making use of the preflight Spectralon reflectance characteristics, vicarious calibrations involving field measurements and AirMISR (MISR's airborne counterpart) [11], and cross-comparisons with other instruments has been invoked in order to meet the required radiometric specifications for the experiment [7], [12].

On February 26 and 27, 2000 the first on-orbit mechanisms tests and calibrations were performed, which consisted of deploying and stowing the two calibration panels and running the goniometer, a swinging arm which enables one set of calibration photodiodes to view the calibration panels over a range of view angles. A set of microswitches intended to indicate that each of the calibration panels had reached the fully deployed position did not activate; however high-rate motor telemetry showed that the panels had indeed deployed and stowed normally. Plots of motor current versus time for the deploy and stow activities of both panels are shown in Fig. 7. Panel motion is associated with a typical current of about 90 mA. When the panel reaches the limit of its motion, the compression of a spring is manifested by a rise in motor current over a period of about 1 s. Following this, the motor stalls and the current rapidly increases to about 270 mA. A computer time-out turns the motor off after a preset stall duration.

The early in-flight tests showed some transients, or "speed bumps," in the current readings for both the north and south panels during the deploy and stow portions of the sequences. These are visible in Fig. 7(a)–(d), and indicate that additional torque above the average level was required to drive the mini-

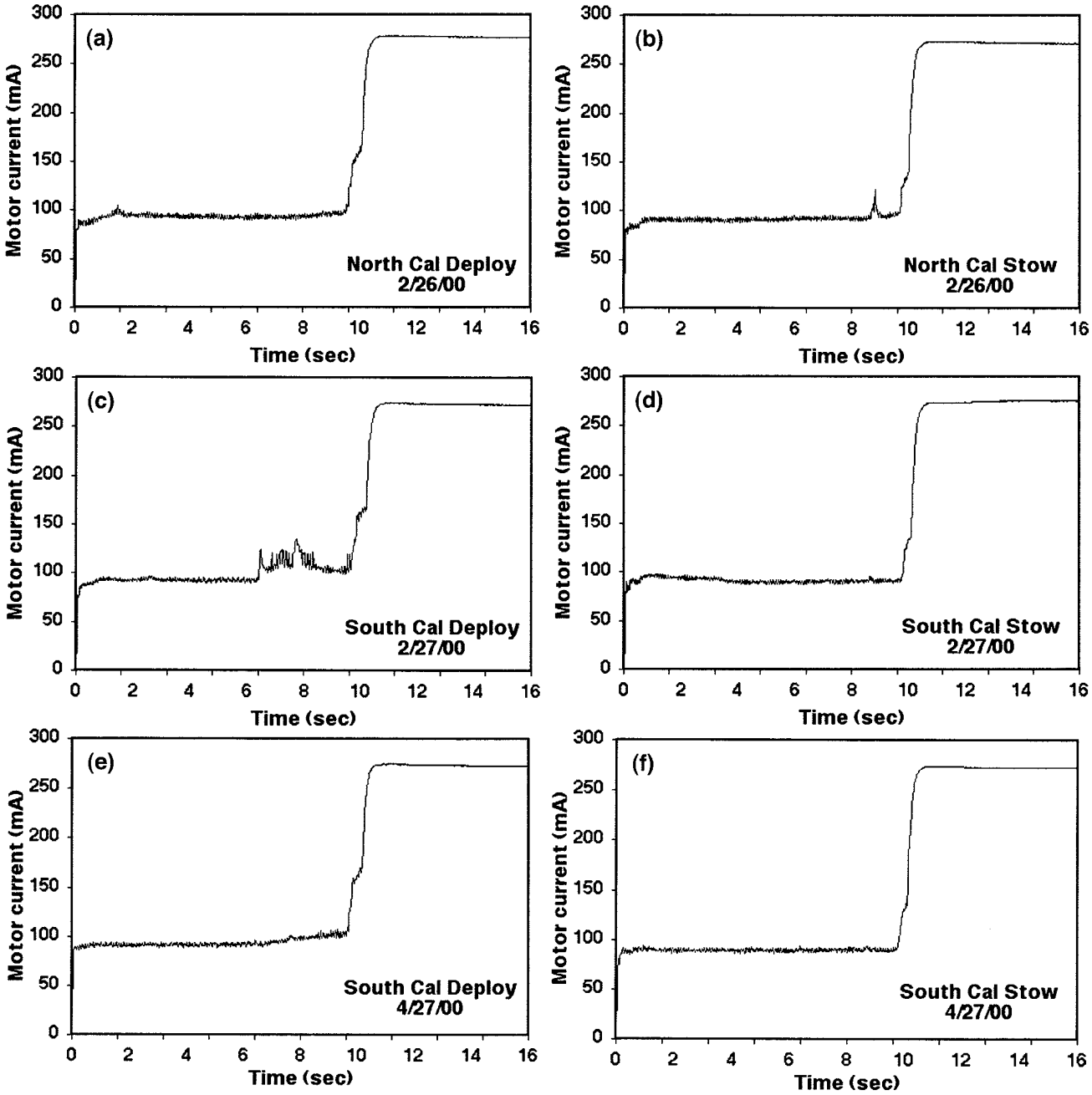

Fig. 7. Plots of motor current during deploy and stow sequences of the north and south calibration panels. (a), (b) Deploy and stow of the north panel on February 26, 2000. (c), (d) Deploy and stow of the south panel on February 27, 2000. (e), (f) Deploy and stow of the south panel on April 27, 2000, after repositioning the goniometer from 0° to +38°.

dual-drive actuators for isolated short intervals. The most worrisome was the transient seen in the south calibration panel deploy curve. Although the current increment was well below design margins and the signature was not consistent with particulate contamination or gear grinding, a moratorium on use of the south calibration panel was put into effect after the first few deployments until the problem was better understood and risks of further use assessed (the calibration panels deploy in front of the cameras, so it is essential for them to re-stow). From the timing of the events, and experimentation with the MISR Engineering Model on the ground, we deduced that certain thermal insulation blankets had "puffed out" slightly in the vacuum of space and some grazing was occurring during the panels' motion. Analysis of the current readings implied that no snagging or binding was occurring. Early calibration sequences with the flight instrument's south calibration panel showed that blanket interference with a metal shield attached to the goniometer could be significantly reduced by repositioning the goniometer to 38° from nadir during south calibration panel motions, instead of the nominal 0° (nadir). The beneficial effect on the motor currents is shown in Fig. 7(e) and (f), for a calibration sequence run on April 27, 2000. This repositioning is now standard operating procedure. For the north calibration panel, the suspected blanket interference had no mitigating solution, and while the observed "speed bumps" are small, there is some possibility that over the long term the polymeric material of the blankets could wear.

Consequently, we decided to reduce the frequency of the north and south calibration sequences to a bimonthly basis, rather than monthly as originally envisioned. After an initial rapid degradation of camera response by about 5% during the first two months after cover open, the measured rate of change has slowed to less than 2% per year. Bimonthly calibrations are therefore quite adequate for maintaining the instrument radiometric scale to within the required accuracy [7].

Five of the nine MISR cameras observe one of the calibration panels during north or south sequences. Ideally, data in each band would be acquired at full resolution (1×1, i.e., no pixel averaging). However, preflight testing showed that the corresponding data rate would cause repeated out-of-sync events. Therefore, the sequences were designed such that pixel averaging was implemented for some channels, and the averaging configuration "toggled" between different channels so that every channel would have the opportunity to acquire data in the 1×1 configuration. Initially, the 1×1 and 4×4 averaging configurations were toggled between the off-nadir A and B cameras. In flight, we discovered that this led to acquisition of insufficient high-resolution data during the important part of the calibration sequence where rapid changes in illumination occur, as the sun is occulted by the earth's atmosphere. A modified sequence took advantage of the fact that the nadir camera views both the north and south calibration panels. For the north calibration sequences, the blue and green bands of the An camera were acquired at full resolution and the red and near-infrared bands were averaged to 4×4, and this was reversed for the south calibration sequences. This approach obviated the need for temporal toggling of averaging configurations between cameras. By uploading a patch to a look-up table, the MISR flight software was able to incorporate modifications to the calibration sequences, and on March 10, 2000 this new approach was implemented.

Two calibration diode sets mounted on the MISR optical bench are oriented at angles corresponding to the off-nadir D cameras. To insure that the radiometric response of these diodes is calibrated to the same scale as the nadir-viewing diodes, the goniometer was used as a transfer between them. Analysis of OBC data acquired during the first year of operations indicated that there was a $\sim$4% bias in the relative calibration of the forward and backward C and D cameras. To cross-check the response of the off-nadir diodes, it was decided to orient the goniometer at the most oblique view angles for a month at a time, using the earth as the illumination source. On May 4, 2001, during an attempt to position the goniometer at $+58^{\circ}$ (the angle required for alignment with one of the off-nadir diode sets), the MISR flight computer was unable to keep up with the extra workload, since generation of high-rate camera data was in process at the time. As a result, the computer ceased updating engineering telemetry packets correctly and also lost track of the IMOK ("I'm OK") "heartbeat" signal from the spacecraft. The latter initiated a transition to Safe Mode. Additionally, one of the spacecraft TMONs detected the failure of the packet counter updates, and the spacecraft issued a command to turn MISR off. Subsequent troubleshooting discovered that software limits establishing the allowable positioning range for the goniometer were not properly set. After establishing the cause of the shutdown, MISR was reactivated on May 8, 2001. This event was the first time instrument power had been recycled since initial turn-on in December 1999. An operational prohibition against moving the goniometer while all cameras are in science mode was established.

D. Optical Quality

The MISR lenses are superachromatic, seven-element, refractive f/5.5 telecentric designs. A double-plate Lyot depolarizer is incorporated into each of the cameras to render them polarization insensitive. Focal lengths vary from 59 mm for the A cameras to 124 mm for the D cameras. This unique design enables cross-track pixel size and sample spacing to be maintained at 250 m for the nadir camera and 275 m for all of the off-nadir cameras. Along-track footprints depend on view angle, ranging from 214 m in the nadir to 707 m at the most oblique angle. However, sample spacing in the along-track direction is 275 m in all cameras as a consequence of the 40.8-msec line repeat time of the CCD readout from each channel. The georectification process resamples the data from all cameras to a 275-m SOM grid.

An illustration of camera optical quality is provided in Fig. 8(a)–(f). These show full resolution red band data from cameras Df, Cf, Af, Ba, Ca, and Da, respectively for a portion of the Virginia and North Carolina coasts. (Images from the other cameras are not shown and would not add substantially to this discussion.) The data were acquired on October 11, 2000 during Terra orbit 4344, and have been cropped to a width of 698 pixels and a length of 324 pixels (i.e., 13.2 s of data from each camera). The images have been radiometrically calibrated, but are not georectified, and show the data in camera line and sample coordinates, i.e., prior to mapping to the SOM projection. Intra- and intercamera geometric distortions have therefore not been removed. A bad line due to an out-of-sync event has been blanked out near the top of the Cf image.

The dark area near the lower left is the Dismal Swamp National Wildlife Refuge, with Lake Drummond at its center. Near the top left, the Chesapeake Bay Bridge–Tunnel is discernible at all angles. The backward views, which look away from sunglint, show this roadway with the highest contrast, and the two segments where it dips underground are clearly visible as gaps. Other bridges can be seen, such as the James River Bridge to the northwest of the Dismal Swamp. Numerous ship wakes show up as bright spots in the water, and are visible in the imagery from multiple cameras. In the forward views, an interesting change in appearance of the sunglint pattern from one angle to another can be seen. Especially noteworthy is the reversal in contrast on the right hand side of the Cf and Af images. A quantitative explanation would require a model of the physical structure on the ocean surface, but we can surmise that these data are revealing information about the orientation and slope of the leading and trailing faces of surface waves. Studies of organic and inorganic suspended matter beneath the water's surface, on the other hand, would be best performed using the backward-viewing cameras.

During prelaunch assembly and testing, measurements of the camera point spread functions (PSF) revealed low-level cross-

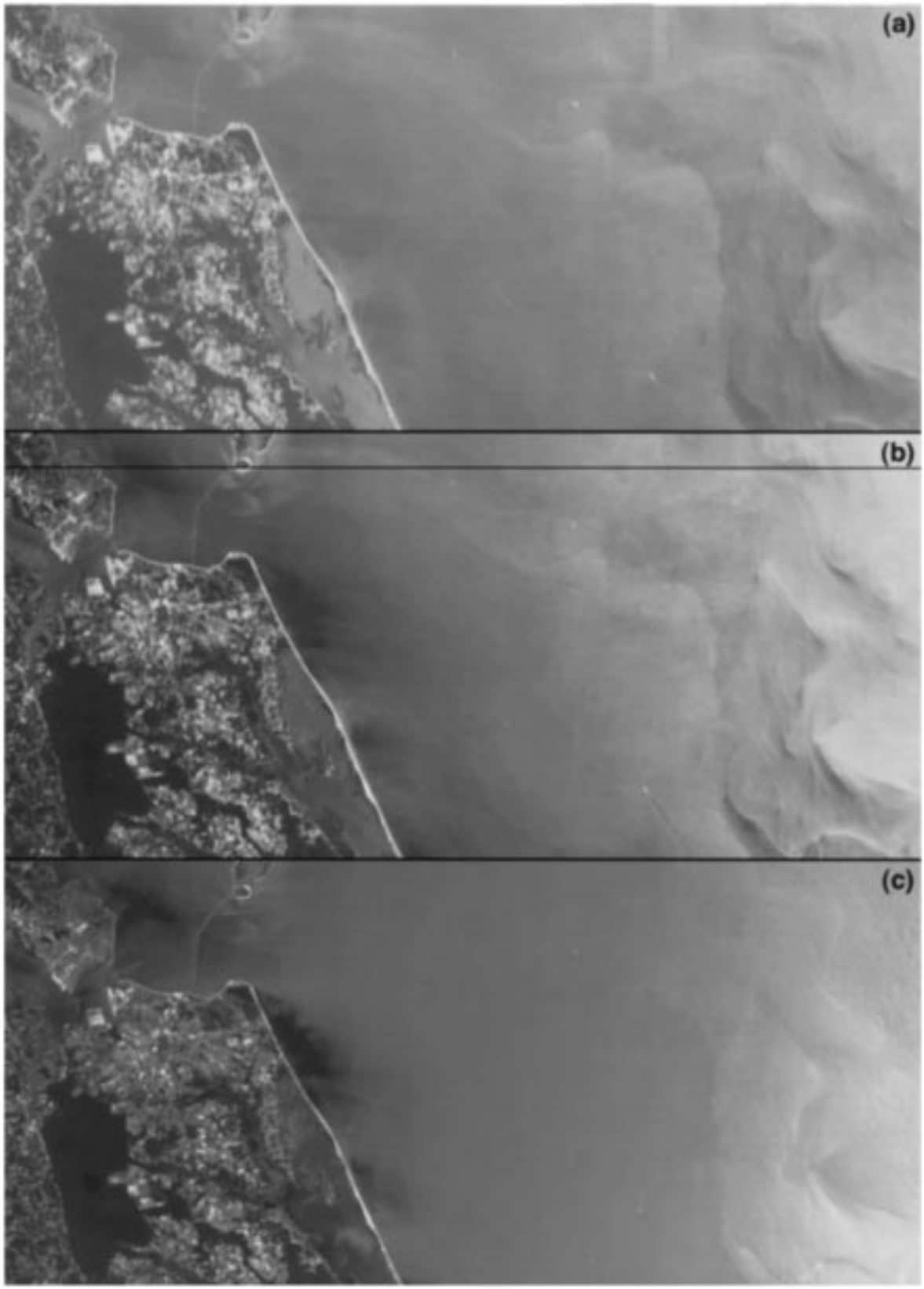

Fig. 8. (a) Radiometrically calibrated image from the red band of the Df camera, from orbit 4344. The data have not been georectified, so each of the 324 lines in the image is in the format obtained from the camera output, except that the data have been cropped to a 698-pixel portion of the full swath width. A nonlinear contrast stretch was applied to highlight features in the image, including several bridges, boat wakes, and brightness variations in the water. (b) Cf camera data. (c) Af camera data.

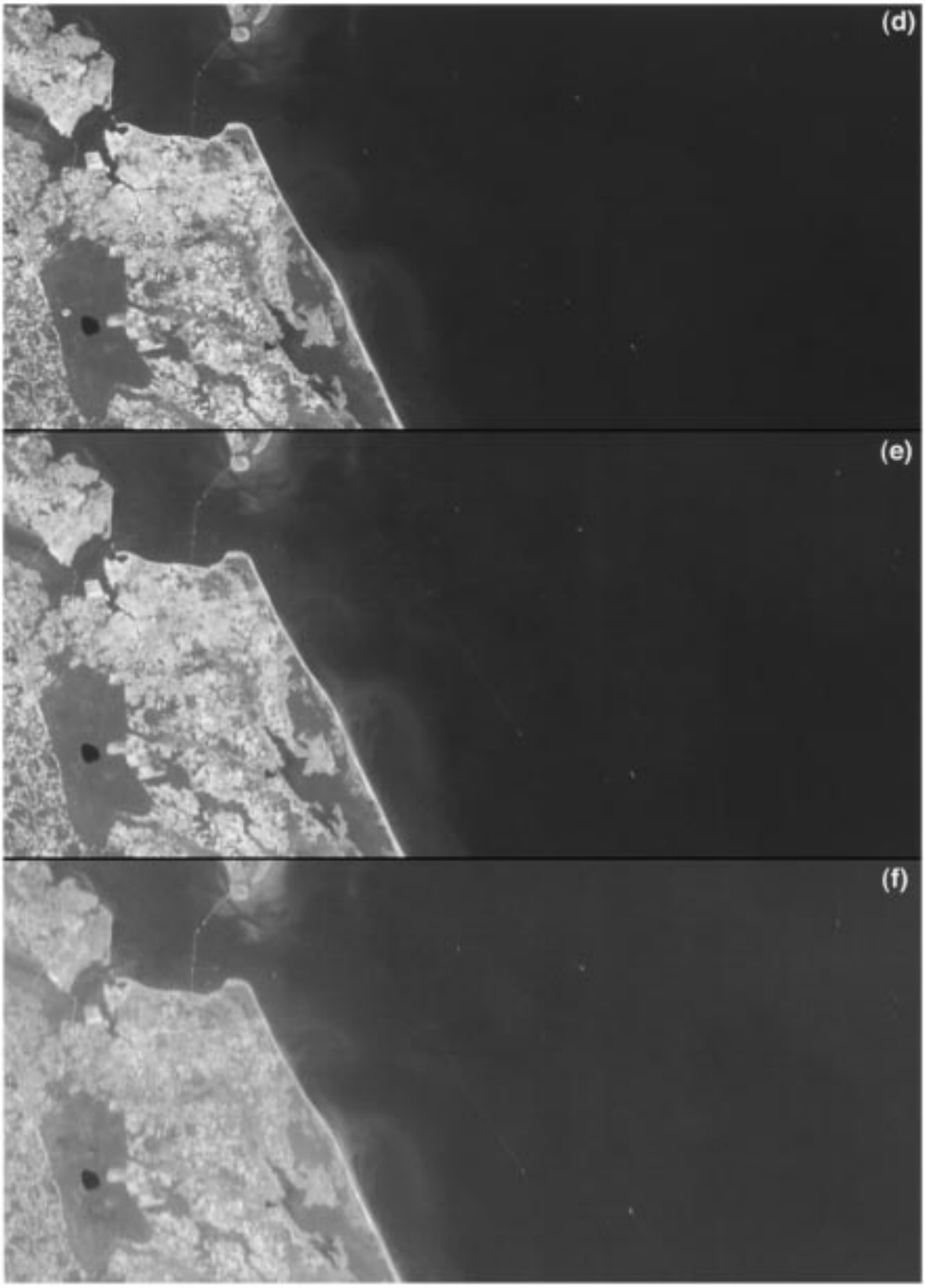

Fig. 8. (*Continued*.) (d) Ba camera data. (e) Ca camera data. (f) Da camera data.

track halos containing a few percent of the encircled energy and extending tens of pixels to either side of the central core. They are believed to arise from scattering between the CCD focal planes and the overlying filters. Recent analyses of in-flight data have also revealed the presence of low-level ghosting, most likely due to reflections between the top surface of the focal plane filters and one or more lens surfaces [7]. For many applications, these scene-dependent effects are not likely to be significant in that they reduce contrast by a few percent; however, for dark ocean scenes with bright areas in the camera fields-of-view, it will be necessary to implement correction procedures in the ground data processing to maintain the desired level of radiometric accuracy. Detailed studies of the in-flight performance are underway, and correction algorithms are being developed. In principle, a PSF deconvolution to account for the change in geometric footprint from one camera to another in the along-track direction is also possible, due to the oversampling along this axis. However, this step is not currently part of routine data processing plans. No PSF or ghosting corrections have been applied to Fig. 8(a)–(f).

E. Geometric Calibration

Early in the Terra mission the spacecraft star trackers were activated, and the GNC subsystem detected a $\sim 0.01^\circ$ jitter in the spacecraft orientation, induced by motion of the HGA. An oscillation by this amount would be just detectable in MISR images (although at the time MISR was not yet acquiring such imagery). Because the oscillation followed a predictable pattern, the spacecraft GNC engineers developed a method of anticipating and compensating for it using Terra's attitude control system. This reduced the magnitude by an order of magnitude, to virtually undetectable levels from a MISR standpoint.

At any one instant, the 36 channels of data from the instrument do not view the same points on the earth; in the most extreme case there is a 2800-km separation between the Df and Da views. Spatial coregistration of the 36 channels of data from the instrument is an essential requirement of all of the MISR geophysical retrievals, and is accomplished during ground data processing [9]. Instrument-related geometric distortions are accounted for by extensive geometric camera calibration. This calibration establishes to high accuracy the along-track camera boresight angles as well as the small cross-track offset angles that are included in the instrument design to compensate for earth rotation during the 7-min interval between the Df and Da views. Use of the preflight camera geometric model was adequate for registering the imagery from the nadir, A, and B, cameras, but multipixel misregistrations were found for the C and D cameras. Using the supplied spacecraft attitude and ephemeris information, and making in-flight refinements to the camera models, the mean geolocation error for eight out of nine cameras was reduced to below 60 m with the standard deviations ranging between 100 m for the nadir view angle to 300 m for the most oblique angles. Coregistration of these cameras has therefore been achieved to within one pixel uncertainty. For reasons not well understood, the Da camera exhibited misregistrations of up to two pixels. Before launch, it was planned to generate a set of cloud-free "reference orbit imagery" (ROI) to which all camera data would be coregistered by supplementing the "dead reckoning" navigation (i.e., use of attitude, ephemeris, and camera geometric model data) with image matching to remove residual distortions. This plan, along with a recalibration of the Da camera geometric model, is being implemented and reduction of residual misregistrations to one pixel or better for all cameras is anticipated [8]. Attaining this accuracy is particularly critical for MISR's stereoscopic cloud height and wind retrievals.

One method of assessing camera coregistration performance and simultaneously visualizing terrestrial angular "signatures" is through the use of "false" color. Traditionally, this approach is used to place spectral bands other than red, green, and blue in the RGB channels of a full-color display. The geometric registration of MISR data as a function of view angle enables placing data from a single spectral band but at different angles into the RGB display channels. Fig. 9(a)–(c) provide an example of this visualization. Fig. 9(a) is a "true" color nadir view of northern Botswana, Africa. True color is taken to mean that data from the red, green, and blue bands are placed in the RGB display channels, respectively, but is not intended to imply that the relative spectral content has been calibrated against a photometric standard. The distinctive fan-like feature is the highly vegetated Okavango Delta, a mosaicked network of grasslands and water channels, observed here during the dry season on August 25, 2000 during Terra orbit 3655. Fig. 9(b) is a spectral false color rendition, in which the nadir green, red, and near-infrared bands are displayed as RGB. Note how the plant life, which is highly reflective in the near-infrared, shows up as bright red in this view. Fig. 9(c) contains red band data only, but is a composite of imagery from the An, Df, and Da cameras displayed as RGB. The color variations in this multiangle composite arise not from how the different parts of the scene reflect light at different wavelengths, but rather, at different angles. Typically, vegetation preferentially reflects light back toward the source of illumination, so in Fig. 9(c), the Df camera image, which is displayed in green, is brighter where vegetation is prevalent. Several smoke plumes show up in distinctive shades of purple in the multiangle composite as a result of the different angular signature of these aerosols relative to the surface. Automated registration of the imagery from widely disparate view angles is performing well, even prior to implementation of the ROI methodology.

F. Flight Software

The MISR flight software is coded in Ada, and the version uploaded at the start of the mission in January 2000 (V3.0.0.2) provided 14 operational modes of the instrument [1]. On May 22, 2001 a new flight software load, V3.0.0.4, was successfully loaded into the MISR instrument. (V3.0.0.3 had been prepared to correct some minor bugs prior to launch, but it was never used, and became superseded by V3.0.0.4.) The new load established an 8-s interval between camera turn-on and exposure time commands (see Section III-A), updated the calibration sequence tables to capture the patch that was implemented in March 2000 (Section III-C), and incorporated software limits that simplified the procedures for positioning the goniometer to $+38^\circ$ for the

Fig. 9. (a) True-color An georectified image of northern Botswana, Africa acquired on August 25, 2000 during Terra orbit 3655. The distinctive fan-like feature is the Okavango Delta. Near the top of the image is the Caprivi Strip, a narrow panhandle in northeast Namibia.

south calibration panel activities (Section III-C). The principal purpose of V3.0.0.4, however, was to define two new instrument modes, Global TAXI Off and Global TAXI On, in order to reduce thermal stresses on the camera electronics boards (Section II-C). Global TAXI Off keeps the cameras powered on the night side but inhibits high-rate data output. At the north terminator, Global TAXI Off transitions to Global TAXI On, which reenables the high-rate data flow for all cameras simultaneously. This is in contrast to the transition from Engineering to Global Mode, where the cameras are turned on sequentially as their views cross the north terminator. Further updates to the flight software are not anticipated at this time.

Fig. 9. (*Continued*.) (b) Camera An false-color infrared image of the same region.

IV. Conclusions

The in-flight performance of the MISR instrument has been excellent. During instrument activation and orbital operations, several anomalies were encountered. Resolution relied extensively on tests and simulations with the MISR Engineering Model (EM), which we regard as a vital contributor to mission success. Budget stresses can lead to pressures to cut costs and dispense with an EM. Based on our experience, we strongly believe that any resultant savings would be of negligible consequence compared to the extraordinary benefit of being able to diagnose an instrument's health remotely from limited telemetry information, and to assess and mitigate risk.

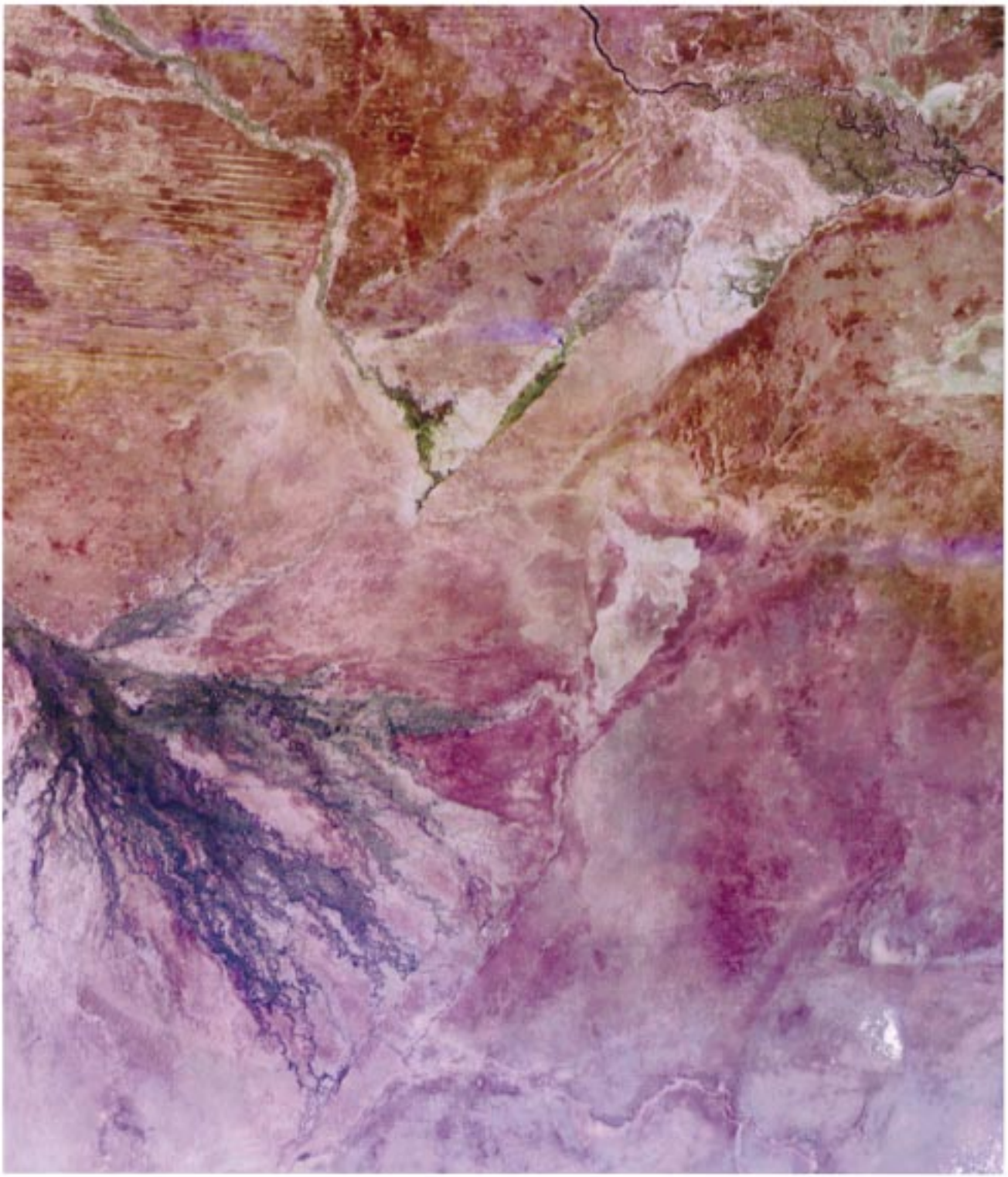

Fig. 9. (*Continued*.) (c) Multiangle composite image of the same region, generated using red band imagery from the An (displayed as red), Df (displayed as green), and Da (displayed as blue) cameras.

As this and other papers in this special issue illustrate, considerable care is being taken by the MISR team to provide high-quality, quantitatively accurate, and well-characterized data for use by the scientific community. As with any new instrument, data type, algorithm, or software package, discoveries regarding product quality occur on an ongoing basis. The research community is encouraged to participate in the process of validating and improving MISR products, as well as in the exploration of new methods to take best scientific advantage of the unique data provided by this experiment. MISR data

products are available to the science community and the public through the NASA Langley Atmospheric Sciences Data Center (ASDC), http://eosweb.larc.nasa.gov. Additional information about the MISR science data system is presented in this issue [13].

For further information about the MISR experiment, the reader is directed to our World Wide Web site at http://www-misr.jpl.nasa.gov. New samples of MISR imagery and/or derived products are posted on the home page every week, and an image archive is accessible via an online gallery. Feedback to the MISR science team is welcome, either through User Services at the ASDC or by e-mailing the MISR project at suggestions@mail-misr.jpl.nasa.gov.

ACKNOWLEDGMENT

The authors gratefully acknowledge the efforts of the entire MISR hardware and software engineering teams. They thank the present and former members of the MISR operations team, S. Barry, H. Fitzhugh, G. Francis, T. Nolan, S. Pick, and P. Varanasi. They also appreciate the efforts of G. Aveni, T. Bickler, L. Hovland, M. Gibbel, M. Johnson, M. Khorrami, D. Peters, A. Rose, and E. Villegas who helped with various phases of the in-flight engineering, operations, and anomaly resolution, and who offered thoughtful and constructive advice. Thanks are also due to MISR's former Experiment and Project Managers, E. Floyd, T. Reilly, and T. Livermore. The authors are grateful for instrument operations support from individuals at the Goddard Space Flight Center, including T. Anderson, K. Grady, J. Kronenwetter, J. Purcell, D. Ramey, C. Scolese, and many others. They appreciate the advice of the JPL board, chaired by D. Swenson that reviewed their plans to upgrade the instrument flight software.

REFERENCES

[1] D. J. Diner, J. C. Beckert, T. H. Reilly, C. J. Bruegge, J. E. Conel, R. A. Kahn, J. V. Martonchik, T. P. Ackerman, R. Davies, S. A. W. Gerstl, H. R. Gordon, J.-P. Muller, R. B. Myneni, P. J. Sellers, B. Pinty, and M. Verstraete, "Multi-angle Imaging SpectroRadiometer (MISR) instrument description and experiment overview," *IEEE Trans. Geosci. Remote Sensing*, vol. 36, pp. 1072–1087, July 1998.

[2] V. R. Taylor and L. L. Stowe, "Reflectance characteristics of uniform Earth and cloud surfaces derived from Nimbus-7 ERB," *J. Geophys. Res.*, vol. 89, p. 4987, 1984.

[3] N. C. M. Stricker, A. Hahne, D. L. Smith, J. Delderfield, M. B. Oliver, and T. Edwards, "ATSR-2: The evolution in its design from ERS-1 to ERS-2," *ESA Bull.*, vol. 83, pp. 32–37, 1995.

[4] P.-Y. Deschamps, F.-M. Bréon, M. Leroy, A. Podaire, A. Bricaud, J.-C. Buriez, and G. Sèze, "The POLDER mission: Instrument characteristics and scientific objectives," *IEEE Trans. Geosci. Remote Sensing*, vol. 32, pp. 598–615, May 1994.

[5] D. J. Diner, G. P. Asner, R. Davies, Y. Knyazikhin, J.-P. Muller, A. W. Nolin, B. Pinty, C. B. Schaaf, and J. Stroeve, "New directions in Earth observing: Scientific applications of multiangle remote sensing," *Bull. Amer. Meteorol. Soc.*, vol. 80, pp. 2209–2228, 1999.

[6] N. L. Chrien, C. J. Bruegge, and R. A. Ando, "Multi-angle Imaging SpectroRadiometer (MISR) On-Board Calibrator (OBC) in-flight performance studies," *IEEE Trans. Geosci. Remote Sensing*, vol. 40, pp. 1493–1499, July 2002.

[7] C. J. Bruegge, N. L. Chrien, R. A. Ando, D. J. Diner, M. C. Helmlinger, W. A. Abdou, and K. Thome, "Early validation of Multi-angle Imaging SpectroRadiometer (MISR) radiometric scale," *IEEE Trans. Geosci. Remote Sensing*, vol. 40, pp. 1477–1492, July 2002.

[8] V. Jovanovic, M. Bull, M. Smyth, and J. Zong, "MISR in-flight camera geometric model calibration and georectification performance," *IEEE Trans. Geosci. Remote Sensing*, vol. 40, pp. 1512–1519, July 2002.

[9] V. M. Jovanovic, M. M. Smyth, J. Zong, R. Ando, and G. W. Bothwell, "MISR photogrammetric data reduction for geophysical retrievals," *IEEE Trans. Geosci. Remote Sensing*, vol. 36, pp. 1290–1301, July 1998.

[10] J. I. Rodriguez and D. J. Diner, "Thermal design and on-orbit performance of the Multi-angle Imaging SpectroRadiometer," in *31st Int. Conf. Environmental Systems, SAE Tech. Paper Series*, July 2001, Paper no. 2001-01-2262.

[11] D. J. Diner, L. M. Barge, C. J. Bruegge, T. G. Chrien, J. E. Conel, M. L. Eastwood, J. D. Garcia, M. A. Hernandez, C. G. Kurzweil, W. C. Ledeboer, N. D. Pignatano, C. M. Sarture, and B. G. Smith, "The Airborne Multi-angle Imaging SpectroRadiometer (AirMISR): Instrument description and first results," *IEEE Trans. Geosci. Remote Sensing*, vol. 36, pp. 1339–1349, July 1998.

[12] W. Abdou, C. Bruegge, M. Helmlinger, J. Conel, S. Pilorz, and B. Gaitley, "Vicarious calibration experiment in support of the Multi-angle Imaging SpectroRadiometer (MISR)," *IEEE Trans. Geosci. Remote Sensing*, vol. 40, pp. 1500–1511, July 2002.

[13] G. Bothwell, E. G. Hansen, R. E. Vargo, and K. C. Miller, "The MISR science data system, its products, tools, and performance," *IEEE Trans. Geosci. Remote Sensing*, vol. 40, pp. 1467–1476, July 2002.

David J. Diner (A'01) received the B.S. degree in physics (with honors) from the State University of New York at Stony Brook in 1973 and the M.S. and Ph.D. degrees in planetary science from the California Institute of Technology, Pasadena, in 1977 and 1978, respectively.

He has been with the Jet Propulsion Laboratory, Pasadena, since 1981. He is currently a Principal Member of the Technical Staff and Leader of the Multi-angle Imaging Science Element in the Earth and Space Sciences Division. He has been involved in numerous NASA planetary and Earth remote-sensing investigations, and is Principal Investigator of the MISR experiment and its airborne counterpart, AirMISR.

Dr. Diner is a member of the American Geophysical Union and the IEEE Geoscience and Remote Sensing Society.

Jewel C. Beckert has been with the Jet Propulsion Laboratory, Pasadena, since 1957. Since then, he has participated in most of the planetary missions carried out by the laboratory, concentrating on assembly, test, and launch of spacecraft. In the 1980s, he contributed to the Hubble Space Telescope as Deputy Manager of the Wide Field/Planetary Camera (WFPC) 1 and 2 Projects. In 1996, he became Deputy Manager and Instrument Manager for the MISR Project. He is now retired but continues to work "on-call."

Graham W. Bothwell received the B.Eng. degree in electronics from the University of Queensland, Brisbane, Australia, in 1967.

He was with NASA's Deep Space Station, Canberra, Australia, from 1967 to 1968. From 1969 to 1985, he was with the Anglo-Australian Observatory, Sydney, Australia, where he was involved in computing and electronics development in support of construction and subsequently operation of the 4-m telescope, becoming Head of Computing. He has been with the Jet Propulsion Laboratory (JPL), Pasadena, since 1985, initially as supervisor of a group developing image processing software for JPL's planetary program. Since 1988, he has worked with various projects associated with NASA's Earth Observing System, and led a group involved in instrument data processing, ground system development, mission operations, and airborne remote sensing. He is currently Manager of the MISR Project.

José I. Rodriguez received the B.S. and M.S. degrees in mechanical engineering from California State University, Northridge, and the Massachusetts Institute of Technology, Cambridge in 1979 and 1981, respectively. He received the Ph.D. degree, also in mechanical engineering, from the University of California, Los Angeles, in 1990.

He has been with the Jet Propulsion Laboratory (JPL), Pasadena, since 1981. He is currently Principal Member of the Technical Staff and Technical Group Leader in the Advanced Thermal and Structural Technology group, Mechanical Systems Engineering and Research Division. His expertise includes advanced thermal and cryogenic technologies such as loop heat pipes, capillary pumped loops, passive multistage coolers, sorption, mechanical and Joule–Thomson cryocoolers, cryogenic heat exchangers, and regenerators. He is currently Cognizant Cryothermal Engineer for several EOS instruments, including MISR, the Atmospheric Infrared Sounder (AIRS), and the Tropospheric Emission Spectrometer (TES). Previously, he was Co-Investigator for the Brilliant Eyes Ten Kelvin Sorption Cryocooler Experiment (BETSCE), which flew aboard the Space Shuttle in 1995.